Photocurrent spectroscopy of optical absorption enhancement in silicon photodiodes via scattering from surface plasmon polaritons in gold nanoparticles

S. H. Lim, W. Mar, P. Matheu, D. Derkacs, and E. T. Yu[a)]
Department of Electrical and Computer Engineering, University of California, San Diego, La Jolla, California 92093-0407

(Received 22 November 2006; accepted 18 March 2007; published online 21 May 2007)

Experimental characterization and finite-element numerical simulations of the electromagnetic interaction between Au nanoparticles positioned atop a Si *pn* junction photodiode and incident electromagnetic plane waves have been performed as a function of wavelength. The presence of the Au nanoparticles is found to lead to increased electromagnetic field amplitude within the semiconductor, and consequently increased photocurrent response, over a broad range of wavelengths extending upward from the nanoparticle surface plasmon polariton resonance wavelength. At shorter wavelengths, a reduction in electromagnetic field amplitude and a corresponding decrease in photocurrent response in the semiconductor are observed. Numerical simulations reveal that these different behaviors are a consequence of a shift in the phase of the nanoparticle polarizability near the surface plasmon polariton wavelength, leading to interference effects within the semiconductor that vary strongly with wavelength. These observations have substantial implications for the optimization of device structures in which surface plasmon polariton resonances in metallic nanoparticles are exploited to engineer the performance of semiconductor photodetectors and related devices. © *2007 American Institute of Physics*.
[DOI: 10.1063/1.2733649]

I. INTRODUCTION

Surface plasmon polaritons[1–3] in metallic nanostructures have been of interest in recent years for a variety of applications in which the large local electromagnetic field arising from the presence of a surface plasmon polariton resonant excitation in the metal, the pronounced forward scattering of incident radiation at wavelengths near the surface plasmon polariton resonance, or related effects are exploited.[4,5] One recent development in this regard has been the demonstration of enhanced optical absorption and photocurrent generation in semiconductor photodiodes induced by scattering from surface plasmon polariton resonances in Au nanoparticles deposited on the photodiode surface[6] and the application of this phenomenon to achieve improved energy conversion efficiency in hydrogenated amorphous silicon thin-film photovoltaic devices.[7] More extensive application and optimization of this phenomenon will require detailed characterization and understanding of the relevant underlying physical mechanisms and their dependence on wavelength, structure, and composition of the metallic nanoparticles, and interaction with the surrounding dielectric environment and underlying semiconductor material.

In this article, we report detailed photocurrent spectroscopy studies of the dependence of this photocurrent enhancement effect on the wavelength of incident radiation combined with finite-element numerical simulations that allow us to elucidate the key physical mechanisms leading to changes in the photocurrent response spectrum as a function of wavelength. The measured change in photocurrent response in a Si *pn* junction photodiode induced by the presence of Au nanoparticles, as a function of the wavelength of incident radiation, is found to agree well with results of finite-element numerical simulations of the change in electromagnetic field amplitude and spatial distribution, and hence, optical transition rate, induced by the Au nanoparticles. Detailed analysis of the computed electromagnetic field distributions reveals that the electromagnetic fields in the semiconductor device region can be interpreted as, approximately, a superposition of the field arising from simple transmission across the dielectric interface formed at the semiconductor surface, and that due to wavelength-dependent scattering by the Au nanoparticle. The phase relationship between these field components can lead to either constructive or destructive interference within the semiconductor, and hence, to either an increase or a decrease in photocurrent response at different wavelengths. This understanding is expected to play an important role in efforts to optimize these effects in different device applications.

II. EXPERIMENT

Si *pn* junction photodiodes were fabricated from 2 in. diam, 300 μm thick, *n*-type Si (001) wafers with resistivity $\rho \approx 3-6\ \Omega$ cm, corresponding to a donor concentration of approximately 10^{15} cm^{-3}. To form the *pn* junctions, B was diffused into the wafers for 15 min at 950 °C under 1000 sccm N_2 in a 3 in. tube furnace. The final sheet resistance of the resulting *p*-type layer was $50-100\ \Omega/\square$, and based on the process parameters employed the B distribution profile was computed analytically[8] and the junction depth was esti-

[a)]Electronic mail: ety@ece.ucsd.edu

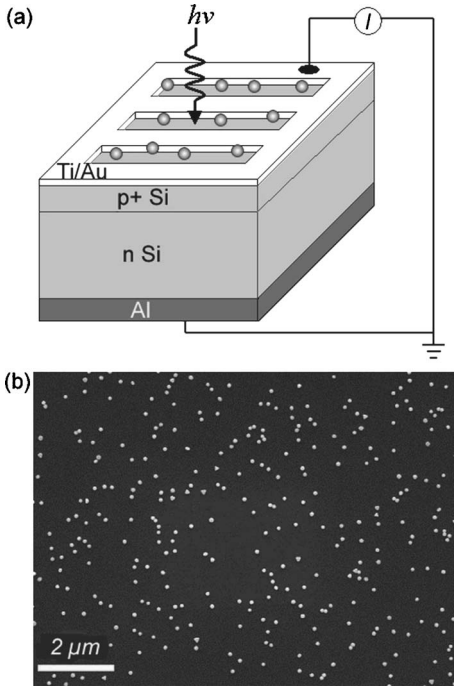

FIG. 1. (a) Schematic diagram of Si *pn* junction photodiode device structure, colloidal Au nanoparticles deposited from solution, and geometry employed for photocurrent response measurements. (b) Scanning electron micrograph of Au nanoparticles deposited on photodiode surface.

mated to be ~0.5 μm. Ohmic contacts to the *p*-type layer were formed in a square grid pattern using 20 nm Ti/80 nm Au metallization in a standard lift-off process and a 200 nm Al film was employed to form a backcontact to the *n*-type layer.

Au nanoparticles were deposited on completed photodiode structures by first coating the device surface with a thin layer of poly-L-lysine, and then depositing several drops of a solution containing colloidal Au nanoparticles 100 nm in diameter onto the device; after 3 min of exposure to the colloidal solution devices were blown dry using nitrogen gas. By repeating the drop deposition and blow drying procedures up to 12 times, particle densities of approximately 3.5×10^8 cm^{-2} on the photodiode surfaces were obtained. While this particle density is well below the density at which photocurrent enhancement effects are expected to be maximized,[7] it is very accessible experimentally and yields sufficiently large changes in photocurrent response for these studies. A schematic diagram of the resulting device structure and a scanning electron micrograph of Au particles on the surface of a representative device, are shown in Fig. 1.

Photocurrent spectra for these devices were obtained using a 50 W tungsten halogen lamp as an illumination source and a grating monochromator with a 600 groove/mm grating, yielding monochromatic light for measurements extending over a wavelength range of 400–1100 nm. For measurements at wavelengths of 600 nm and longer, a red filter was employed to eliminate illumination from the second-order diffraction line. Illumination was incident normal to the surface of the photodiode through a chopper operating at 338 Hz and for all measurements the beam was aligned as close as possible to the center of the device. The resulting photocurrent

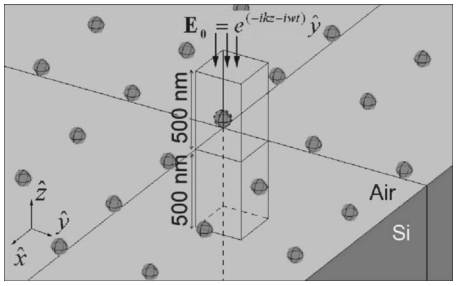

FIG. 2. Schematic diagram of simulation geometry employed. The volume simulated explicitly consisted of the box shown in the figure, with the boundary conditions specified leading the simulations to correspond to an infinite square array of spheres atop a Si substrate.

generated in the device was fed to a lock-in amplifier to isolate the signal component arising specifically from the incident illumination. A 50/50 beam splitter was used to divert part of the light beam emerging from the monochromator to a Si photodiode, the output of which was fed to second lock-in amplifier to detect and compensate for variations or possible drift in incident illumination intensity. The photocurrent spectra shown in Sec. IV have been normalized to account for the source illumination spectrum measured in this manner.

To obtain the most precise possible measurements of changes in photocurrent response arising from the presence of the Au nanoparticles, the following particle deposition and measurement procedures were employed. First, a layer of poly-L-lysine was deposited on the surface of a photodiode device and a reference photocurrent spectrum, $I_{\mathrm{ref}}(\lambda)$, for the device was obtained in the manner described earlier. Au nanoparticles were then deposited on the same device and a second photocurrent spectrum, $I_{\mathrm{np}}(\lambda)$, measured in the presence of the nanoparticles. The ratio $I_{\mathrm{np}}/I_{\mathrm{ref}}$ was then computed to determine the influence of the Au nanoparticles on photocurrent response as a function of wavelength. The reference spectrum $I_{\mathrm{ref}}(\lambda)$ was obtained subsequent to deposition of the poly-L-lysine layer, as the presence of this layer was found to cause a slight change in the spectral response of the photodiode.

III. SIMULATION

Numerical simulations of the electromagnetic field distributions in device structures with and without Au nanoparticles were performed using the FEMLAB$^{\mathrm{TM}}$ finite-element simulation software package with the electromagnetics module. For simulations of devices with Au nanoparticles, the simulation volume consisted a box with dimension L in the x and y directions and Z=1000 nm in the z direction containing a single Au sphere, the bottom of which was separated by 2 nm from a silicon substrate, with boundary conditions specified so as to yield an electromagnetic field distribution corresponding to an infinite array of such spheres, as shown in Fig. 2. Furthermore, specification of the appropriate boundary conditions allows even the single sphere and silicon substrate contained explicitly in this geometry to be simulated by only one quarter their entire volume, corre-

sponding to the region in Fig. 2 for which $0 \leq x \leq L/2$, $0 \leq y \leq L/2$, and $-500\ \text{nm} \leq z \leq 500\ \text{nm}$.

The boundary conditions for this volume are specified as follows. A source term $\mathbf{E}_0 = e^{-ikz}\hat{\mathbf{y}}$, corresponding to a plane wave in the $-z$ direction with unity amplitude, is introduced at the top boundary ($z=500$ nm). No incoming wave, i.e., $\mathbf{E}_0 = 0$, is assumed at the bottom boundary ($z=-500$ nm). The top and bottom boundaries of the simulation volume are constrained in our simulations to satisfy first-order absorbing boundary conditions[9] ($\mathbf{n} \times \nabla \times \mathbf{E} - i\mathbf{k} \cdot \mathbf{E}_{\parallel} = \mathbf{E}_0$) to approximate the effect of an infinite space above the particle and an infinite substrate below the particle.

For the boundary planes $y=0$ and $y=L/2$, we assume $\mathbf{n} \times \mathbf{E} = 0$, where $\mathbf{n}$ is the normal vector to the boundary surface. For the boundary planes $x=0$ and $x=L/2$, we assume $\mathbf{n} \times \mathbf{H} = 0$. These constraints applied to the two boundaries bisecting the sphere, i.e., the planes $x=0$ and $y=0$, cause the fields to be mirrored on the opposing sides. This symmetry is valid because the sphere-substrate system can generate only scattered fields of such symmetry. The boundary conditions applied to the planes $x=L/2$ and $y=L/2$ effectively create a periodic structure corresponding to an infinite array of spheres above a silicon surface, as shown in Fig. 2.

To verify the correctness of these boundary conditions, we analyzed the mathematical solution for light scattering by the sphere-substrate system. We first note that, according to Mie theory,[3] the scattered fields $\mathbf{E}_{\text{sca}}$, $\mathbf{H}_{\text{sca}}$ for a free particle can be decomposed into a series of vector spherical harmonics $\mathbf{M}_{emn}$, $\mathbf{N}_{emn}$, $\mathbf{M}_{omn}$, $\mathbf{N}_{omn}$, where $N=1, 2\ldots$ and $m=\pm 1, \pm 2\ldots$. For excitation by a plane wave polarized in the x direction, only terms $\mathbf{N}_{emn}$, $\mathbf{M}_{omn}$, and $m=$odd exist in $\mathbf{E}_{\text{sca}}$ and only terms $\mathbf{N}_{omn}$, $\mathbf{M}_{emn}$, and $m=$odd for $\mathbf{H}_{\text{sca}}$. These terms generate electric and magnetic fields such that $\mathbf{n} \times \mathbf{E} = 0$ at the $x=0$ plane and $\mathbf{n} \times \mathbf{H} = 0$ at the $y=0$ plane. For our simulations, $\mathbf{E}_0$ is taken to be polarized in the y direction and so the earlier conditions should be switched for x and y. However, for the mathematical analysis of our boundary conditions we will continue to assume that $\mathbf{E}_0$ is polarized in the x direction.

For the sphere-substrate system, we employ an approach[10,11] in which the solution for $\mathbf{E}_{\text{sca}}$ is calculated self-consistently, taking into account multiple scattering between the sphere and the substrate. The solution is expressed in terms of Debye potentials, which can be expanded into a multipole series. The multipole terms can be easily transformed into vector spherical harmonics.[12] Therefore, by studying the coefficients of the expanded Debye potentials we find that only terms $\mathbf{N}_{emn}$, $\mathbf{M}_{omn}$, and $m=$odd exist in the solution for $\mathbf{E}_{\text{sca}}$ and only terms $\mathbf{N}_{omn}$, $\mathbf{M}_{emn}$, and $m=$odd for $\mathbf{H}_{\text{sca}}$. Therefore, even in the sphere substrate system the boundary conditions at $x=0$ and $y=0$ are valid. It should be noted that Ref. 10 only lists the solution for the fields in the region above the substrate. However, a simple extension to their analysis yields the solution for the substrate region as well.

To verify the boundary conditions employed for the planes $x=L/2$ and $y=L/2$, we first consider scattering from two particles, one at the origin (0, 0) and the other at $(x, y)=(L, 0)$. These particles produce scattered fields of the form

$$\mathbf{E}_{\text{sca}}^{(0,0)} = \sum_{\substack{n=1, \\ m=\text{odd}}}^{\infty} a_n \mathbf{N}_{emn}^{(0,0)} + b_n \mathbf{M}_{omn}^{(0,0)}, \tag{1}$$

$$\mathbf{E}_{\text{sca}}^{(L,0)} = \sum_{\substack{n=1, \\ m=\text{odd}}}^{\infty} a_n \mathbf{N}_{emn}^{(L,0)} + b_n \mathbf{M}_{omn}^{(L,0)}. \tag{2}$$

Adding these fields together, we find that any electric field parallel to the $x=L/2$ plane will be canceled out at the plane, and therefore $\mathbf{n} \times \mathbf{E} = 0$ at $x=L/2$. By considering a pair of particles at (0, 0) and $(0, L)$, a similar argument can be made for the $\mathbf{H}$ field, and hence, $\mathbf{n} \times \mathbf{H} = 0$ at $y=L/2$. The particle pair example can now be extended to an infinite array with the same consequences for the boundaries at $x=L/2$ and $y=L/2$.

For the full system including the sphere, substrate, and infinite array condition, we combine the theory of Ref. 10 with the theory for multiple scattering between particles.[13] We write the final solution as a sum of terms $\mathbf{E}_{\text{sca}}^{(0,0)}$, $\mathbf{E}_{\text{sca}}^{(L,0)}$, $\mathbf{E}_{\text{sca}}^{(0,L)}$, $\mathbf{E}_{\text{sca}}^{(2L,0)}$, etc. Because each particle reflects radiation incident upon it, we need to consider what happens when radiation from an infinite array is incident on the particle at (0, 0). In particular, we must determine whether such radiation will cause the particle to generate terms in $\mathbf{E}_{\text{sca}}^{(0,0)}$ that are not in the space of $\mathbf{N}_{emn}$, $\mathbf{M}_{omn}$, and $m=$odd. Using the scalar addition theorem[14] to expand the contribution to the electric fields from all the particles not at the origin, together with the theory of Ref. 10 to calculate the response of the particle at (0, 0) to this radiation, we find that $\mathbf{E}_{\text{sca}}^{(0,0)}$ retains the form of Eq. (1). A similar argument can be applied for the magnetic fields.

These boundary conditions are then employed in the solution of the vector Helmholtz equation ($\nabla \times \nabla \times \mathbf{E} - k^2 \mathbf{E} = 0$) within the simulation volume. In the finite element method, this problem is discretized by dividing the total simulation volume into small volume elements and converting the differential equation into a system of linear equations. Typically our simulations contained approximately 500 000 elements, corresponding to a typical dimension for each element of $\sim\lambda/5$ or smaller, where λ is the wavelength of the electromagnetic field in the simulation. Due to memory constraints, solutions were generally obtained using an iterative solver. For the results presented, all solutions converged with a residue $r < 10^{-6}$. The wavelength-dependent dielectric functions for Au and Si were obtained from Ref. 15.

IV. RESULTS AND DISCUSSION

The photocurrent response spectrum of a reference Si *pn* junction photodiode device, $I_{\text{ref}}(\lambda)$, and the ratio $I_{\text{np}}(\lambda)/I_{\text{ref}}(\lambda)$ of the photocurrent response spectrum of a device functionalized with Au nanoparticles, $I_{\text{np}}(\lambda)$, to the reference spectrum are shown in Fig. 3. The reference spectrum exhibits the expected increase in photocurrent response as

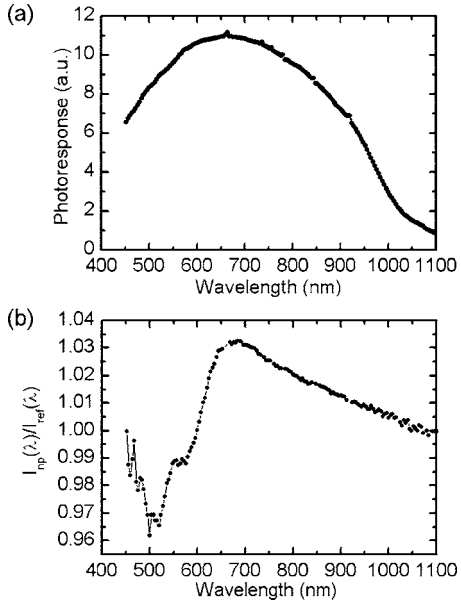

FIG. 3. (a) Measured photocurrent response spectrum of a Si *pn* junction photodiode, $I_{ref}(\lambda)$, without Au nanoparticles. (b) Ratio of the photocurrent response of a Si *pn* junction photodiode upon which Au nanoparticles have been deposited, $I_{np}(\lambda)$, to that of the same device prior to nanoparticle deposition, $I_{ref}(\lambda)$.

the wavelength decreases from the value corresponding to the Si energy band gap (~1100 nm). The decrease in photocurrent response with decreasing wavelength that occurs between approximately 400 and 650 nm is an expected consequence of surface recombination of carriers generated near the surface by short-wavelength photons.[16]

The measured ratio of the reference and nanoparticle-functionalized device photocurrent response spectra shown in Fig. 3(b) exhibits a peak at a wavelength of approximately 680 nm, with a long tail extending to nearly 1100 nm. The peak in the extinction spectrum of the 100 nm diameter Au nanoparticles employed here, corresponding to the surface plasmon polariton resonance wavelength, has been measured previously to be at approximately 600 nm for nanoparticles suspended in aqueous solution.[6] Given the difference in local dielectric environment in the current experiment relative to aqueous solution, a slight shift in surface plasmon polariton resonance wavelength would not be unexpected. In addition, as discussed in detail later, the peak in the photocurrent response spectrum is actually expected to be shifted to somewhat longer wavelengths relative to the surface plasmon polariton resonance—as we observe. The observation of increased photocurrent response over a broad range of wavelengths extending from the peak in $I_{np}(\lambda)/I_{ref}(\lambda)$ at ~680 nm to nearly 1100 nm can be attributed to scattering of the incident light by the Au nanoparticles. For Au nanoparticles with diameter ~100 nm or larger, the dominant interaction between incident radiation at wavelengths near and longer than the surface plasmon polariton wavelength is scattering, which occurs predominantly in the forward direction. Thus, the increased photocurrent response induced by the Au nanoparticles in this wavelength range is attributed to forward scattering of the incident light into the semiconductor photodiode active region.[7]

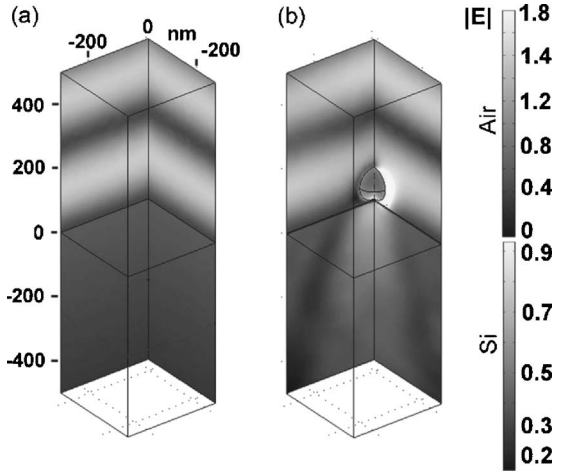

FIG. 4. Grey-scale images of electric field magnitude $|\mathbf{E}|$, obtained from finite-element numerical simulations, for an electromagnetic plane wave with wavelength 550 nm incident on (a) a Si semiconductor substrate and (b) a Si semiconductor substrate with a 100 nm diameter Au nanoparticle positioned 2 nm above the Si surface.

At wavelengths below approximately 650 nm, a pronounced drop in $I_{np}(\lambda)/I_{ref}(\lambda)$ is observed, such that at wavelengths below ~600 nm the presence of the Au nanoparticles leads to a decrease in the observed photocurrent response. Finite-element numerical simulations were employed to elucidate the origin of this behavior. Figure 4 shows the amplitude of the electric field, $|\mathbf{E}|$, computed for an electromagnetic plane wave with a wavelength of 550 nm incident on a Si substrate, and on a Si substrate with a 100 nm diameter Au sphere located 2 nm above the Si surface. The dimensions of the volume simulated are $300\ \text{nm} \times 300\ \text{nm} \times 1000\ \text{nm}$, so that the simulation results correspond to the behavior of a square array of Au nanoparticles placed atop the Si substrate with periodicity of 600 nm in the x and y directions, corresponding to a nanoparticle density of $2.78 \times 10^8\ \text{cm}^{-2}$—close to but slightly less than the density of $\sim 3.5 \times 10^8\ \text{cm}^{-2}$ in our experiments.

From Fig. 4(b), we see that the dipolar surface plasmon polariton resonance mode in the Au nanoparticle gives rise to an increased field amplitude to the immediate right of the particle and a decreased amplitude to the left. In addition, the region of increased field amplitude extending into the Si substrate below the particle—absent in the simulation without the Au nanoparticle—is clearly evident and confirms the effect of strong forward scattering by the particle on the field amplitude within the Si substrate. The oscillations in field amplitude above the Si surface in both cases arise due to nonzero reflection of the incident electromagnetic field at the Si surface.

To estimate the influence of the nanoparticle-induced changes in electric field amplitude on photocurrent generation in a photodiode, we note that electromagnetic radiation incident on a semiconductor gives rise to an optical transition rate, and consequently electron-hole pair generation rate, proportional to the electric field amplitude squared within the semiconductor. Thus, integration of the square of the electric field amplitude computed in our simulations over the semiconductor volume is expected to provide a measure of the

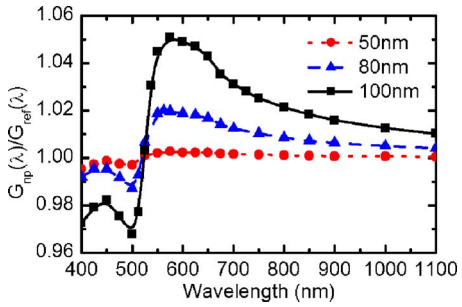

FIG. 5. (Color online) Simulated electric field amplitude squared, $|\mathbf{E}|^2$, integrated over the semiconductor volume for electromagnetic plane waves incident on Si with Au nanoparticles 50, 80, and 100 nm in diameter placed atop the Si surface. All integrated quantities G_{np} are normalized to the integral of $|\mathbf{E}|^2$ for a Si substrate in the absence of any Au nanoparticles, G_{ref}.

photocurrent generated by the incident radiation in each of the simulations, assuming unity efficiency in collection of photogenerated carriers to produce electrical current. Letting G_{ref} refer to the integrated electric field amplitude squared in the silicon region for the reference simulation structure consisting only of air and the Si substrate, and G_{np} to the corresponding quantity for the simulation structure containing air, the Si substrate, and the Au nanoparticle, the ratio G_{np}/G_{ref} should then yield an estimate of the expected increase in photocurrent response in a semiconductor photodiode due to the presence of Au nanoparticles at the simulated particle density.

Figure 5 shows the ratio G_{np}/G_{ref} computed for the geometry shown in Fig. 4 as a function of the wavelength of incident radiation for Au nanoparticles 50, 80, and 100 nm in diameter. For 100 nm diameter Au nanoparticles, we see very clearly a structure highly reminiscent of that observed experimentally in the normalized photocurrent response spectrum shown in Fig. 3(b). The maximum increase in simulated response G_{np}/G_{ref} occurs at approximately 580 nm, compared to a peak improvement in response at ~680 nm observed experimentally, with a long-wavelength tail for which increased photocurrent response is expected extending to 1100 nm and possibly beyond—very consistent with experimental observations. The simulations also yield a somewhat larger peak increase in photocurrent response than that observed experimentally—~5% in simulation compared to ~3.3% in our experiments.

The shift in the wavelength at which the maximum nanoparticle-induced photocurrent response increase is observed is believed to be a consequence of the slightly different local dielectric environment of the Au nanoparticle in the simulation compared to that likely to be realized experimentally. In the simulation, the Au particle is assumed to be surrounded by vacuum, with its lowest point 2 nm above the Si surface. Experimentally, it is very likely that a native oxide layer and a thin layer of poly-L-lysine are present above the Si surface and in contact with the Au nanoparticle, increasing the dielectric constant of the region immediately surrounding the Au nanoparticle from that of vacuum, and also increasing the separation between the Au nanoparticle and the semiconductor. Indeed, simulations of structures in which a 30 nm thick dielectric layer with a representative

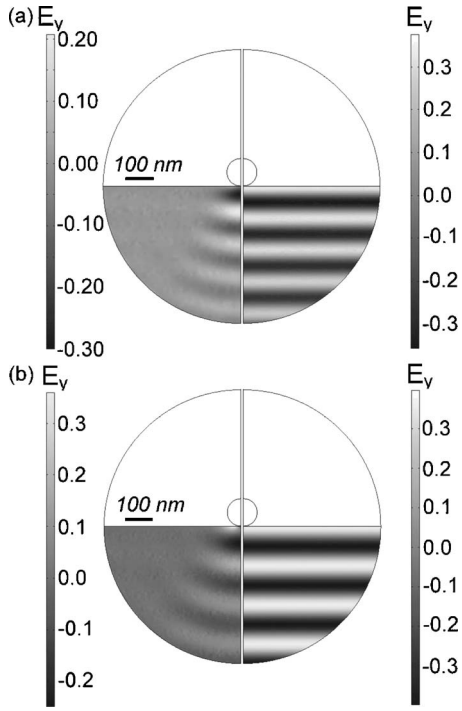

FIG. 6. Simulated y component of the electric field, E_y, in the Si semiconductor region of a structure consisting of a 100 nm diameter Au nanoparticle atop the Si region, separated into components corresponding to transmission across the air-Si interface (lower right quadrants), and scattering from the Au nanoparticle (lower left quadrants), for incident electromagnetic radiation at wavelengths of (a) 500 and (b) 575 nm.

dielectric constant $\varepsilon=3\varepsilon_0$ is included between the Au nanoparticle and the Si surface support the conjecture that the presence of such a dielectric layer should both shift the peak in $I_{np}(\lambda)/I_{ref}(\lambda)$ to longer wavelengths as well as reduce its maximum value.

We also note the occurrence of a decrease in G_{np}/G_{ref} at short wavelengths, with a structure very similar to that observed experimentally in $I_{np}(\lambda)/I_{ref}(\lambda)$. These results demonstrate that the presence of the Au nanoparticle can decrease the electric field amplitude in the substrate as well as increase it. The prediction of large electric fields in the semiconductor due to the surface plasmon polariton resonant mode in the Au nanoparticle alone does not explain this effect—it is necessary in this case to examine both the field scattered from the Au nanoparticle as well as that transmitted directly into the substrate through the dielectric interface formed at the semiconductor surface. To this end, Au nanoparticles that are small compared to the wavelength of incident radiation that may be considered, to a good approximation, point dipoles which are excited by an incident plane wave, and in turn reradiate (or scatter) a portion of the incident power as circular dipole waves—essentially behaving as optical dipole antennas. Thus, the total field inside the substrate can be viewed, approximately, as the superposition of the component of the incident plane wave transmitted across the Si surface into the substrate, and the circular dipole waves scattered from the nanoparticle.

Figure 6 shows, for incident radiation wavelengths of 500 and 575 nm, the computed electric field amplitudes in the substrate region in the presence of a 100 nm diameter Au

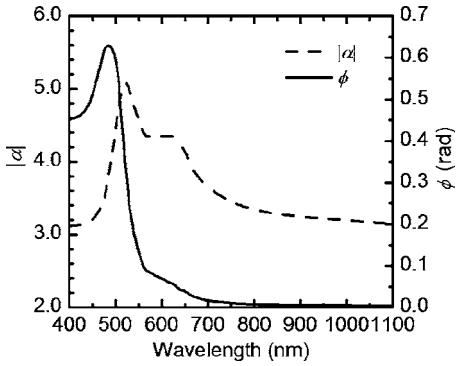

FIG. 7. Magnitude $|\alpha|$ and phase φ of the polarizability $\alpha \equiv |\alpha| e^{i\varphi}$ of a spherical Au particle, normalized to the particle volume $4\pi a^3/3$, as functions of wavelength.

nanoparticle, separated into two components: the plane wave transmitted across the Si surface, as determined from calculating normal plane wave transmission into a dielectric, and the remaining electric field amplitude following subtraction of the transmitted plane wave, corresponding to the circular dipole wave. We note that at 575 nm, the circular dipole wave and the transmitted plane wave are nearly in phase, resulting in constructive interference and a substantial increase in local and integrated electric field intensity, as shown in Fig. 5. In contrast, at 500 nm the circular dipole wave and the transmitted plane wave are no longer in phase, resulting in partial destructive interference and, consequently, a reduction in local and integrated electric field intensity, also evident in Fig. 5. Thus, we see that a key factor in determining whether the integrated field intensity, and consequently photocurrent response in a semiconductor photodiode functionalized with Au nanoparticles, is increased or decreased is the phase relationship between the transmitted and scattered electromagnetic wave components.

The origin of this phase shift can be understood using the quasistatic theory of dipole radiation from spherical particles. An electromagnetic wave incident on a spherical particle with dielectric constant ε surrounded by vacuum excites a dipolar oscillation in the particle which is polarized in the direction of the incident electric field $\mathbf{E}_0(t)$. The polarization of the particle is given by $\mathbf{P}=\alpha\mathbf{E}_0$, where the polarizability α for a spherical particle is given by[3]

$$\alpha = 4\pi a^3 \left(\frac{\varepsilon - \varepsilon_0}{\varepsilon + 2\varepsilon_0} \right).$$

The field scattered from the particle can be considered to be the radiation from this time-dependent polarization. In general, α is complex and can exhibit a pronounced wavelength dependence, as shown in Fig. 7 for a Au particle. Thus, the phase of the particle polarization $\mathbf{P}$, and therefore of the scattered field, which is directly proportional to $\mathbf{P}$, relative to $\mathbf{E}_0$, will be nonzero and wavelength-dependent as well. This phase shift leads to the behavior shown in Fig. 6, in which the scattered field can be either in phase or significantly out of phase with the transmitted field. Specifically, we observe from Fig. 7 that there is a large shift in the phase of α near the surface plasmon polariton wavelength. At ~500 nm and below, corresponding to wavelengths below the surface plasmon polariton resonance, α has a significant nonzero phase, leading to a phase shift between the scattered and transmitted field as shown in Fig. 6(a) for incident radiation at 500 nm. Above ~560 nm, corresponding to wavelengths above the resonance, the imaginary component of α is much smaller, so that at longer wavelengths the scattered and transmitted fields are nearly in phase, as shown in Fig. 6(b) for incident radiation at 575 nm. To assess the validity of the approximation employed in this model, we have also computed exact absorption and scattering cross sections for Au particles 100 nm in diameter in free space over the wavelength range of interest using Mie theory[3] and have confirmed that the dominant contributions arise from the lowest-order, dipole-like mode. For different materials or for particles larger relative to the wavelength, the dipole approximation may not be sufficient, but we expect the general phase and interference phenomena described above to remain relevant.

Because the phase of the scattered field is a key factor in determining the electromagnetic field amplitude within the semiconductor substrate for the device geometry shown in Fig. 1, a detailed understanding and optimization of this aspect of the electromagnetic interaction between a metal nanoparticle, underlying substrate, and incident radiation is essential in optimization of this effect for device applications. For example, for applications such as multispectral imaging, the ability to engineer enhancement of photocurrent response at certain wavelengths while suppressing it at others is likely to be quite useful. For other applications such as photovoltaics, enhancement of photocurrent response over a very broad range of wavelengths is desired and for optimal performance the wavelength range for which photocurrent response is reduced should be shifted so as not to overlap with the incident radiation spectrum of interest.

V. CONCLUSIONS

In summary, we have performed experimental characterization and numerical simulations of the electromagnetic interaction between Au nanoparticles deposited on a Si semiconductor *pn* junction photodiode structure and incident electromagnetic radiation as a function of wavelength, to assess and interpret the degree to which photocurrent response in the semiconductor can be engineered and increased by the presence of the nanoparticles. The presence of Au nanoparticles at a density of $\sim 3 \times 10^8$ cm^{-2} is found experimentally to lead to increased photocurrent response at wavelengths of ~600 nm to over 1000 nm, but to a reduction at wavelengths below 600 nm. Similar behavior is observed in numerical simulations, in which the square of the electric field magnitude, integrated over the entire semiconductor volume, is employed as a proxy for photocurrent response. Furthermore, detailed analysis of the electromagnetic field distribution as a function of wavelength has revealed that the phase relationship between the component of the electromagnetic field transmitted across the Si surface and that scattered by a Au nanoparticle is the key factor in determining whether photocurrent response at a particular wavelength is increased or reduced. Specifically, at wavelengths below the nanoparti-

cle's surface plasmon polariton resonance wavelength, the nanoparticle's polarizability has a significant nonzero phase, leading to destructive interference between the transmitted and scattered field components, and consequently a reduction in photocurrent response, as observed both experimentally and in simulation. At wavelengths above the resonance, the phase of the nanoparticle's polarizability approaches zero, leading to constructive interference of the transmitted and scattered field components and therefore an increase in photocurrent response, again consistent with both experimental and simulation results. This line of reasoning might seem to indicate that the layer of nanoparticles is similar to an antireflection coating. However, we point out that the field enhancement due to an antireflection coating is uniform throughout the semiconductor region, whereas for the case of the nanoparticles, the field enhancement originates from pockets of high field intensities underneath the particles. This might be advantageous for certain solar cell structures where such nonuniform fields can lead to improved optical absorption and photocurrent generation. This understanding also has significant implications for the design of other device structures in which metallic nanoparticles might be employed to engineer various aspects of semiconductor photodetector response.

ACKNOWLEDGMENTS

Part of this work was supported by a grant from the UCSD Von Liebig Center and through the University of California CLC program. S.H.L. would like to acknowledge valuable discussions with J. H. Chung concerning the definition of appropriate boundary conditions in the simulations presented here.

[1] J. P. Kottmann, O. J. F. Martin, D. R. Smith, and S. Schultz, Opt. Express **6**, 213 (2000).
[2] K. L. Kelly, E. Coronado, L. L. Zhao, and G. C. Schatz, J. Phys. Chem. B **107**, 668 (2003).
[3] C. F. Bohren and D. R. Huffman, *Absorption and Scattering of Light by Small Particles* (Wiley, New York, 1983), pp. 93, 100–103, 139.
[4] T. W. Ebbesen, H. J. Lezec, H. F. Ghaemi, T. Thio, and P. A. Wolff, Nature (London) **391**, 667 (1998).
[5] J. A. Porto, F. J. Garcia-Vidal, and J. B. Pendry, Phys. Rev. Lett. **83**, 2845 (1999).
[6] D. M. Schaadt, B. Feng, and E. T. Yu, Appl. Phys. Lett. **86**, 063106 (2005).
[7] D. Derkacs, S. H. Lim, P. Matheu, W. Mar, and E. T. Yu, Appl. Phys. Lett. **89**, 093103 (2006).
[8] J. D. Plummer, M. D. Deal, and P. B. Griffin, *Silicon VLSI Technology* (Prentice-Hall, Upper Saddle River, NJ, 2000), Chap. 7.
[9] J. Jin, *The Finite Element Method in Electromagnetics* (Wiley, New York, 1993), p. 429.
[10] P. A. Bobbert and J. Vlieger, Physica A **137**, 209 (1986).
[11] J. H. Kim, S. H. Ehrman, G. W. Mulholland, and T. A. Germer, Proc. SPIE **4449**, 281 (2001).
[12] C. J. Bouwkamp and H. B. G. Casimir, Physica E (Amsterdam) **20**, 539 (1954).
[13] J. H. Bruning and Y. T. Lo, IEEE Trans. Antennas Propag. **AP-19**, 378 (1971).
[14] W. C. Chew, J. Electromagn. Waves Appl. **6**, 133 (1992).
[15] E. D. Palik, *Handbook of Optical Constants of Solids* (Academic, San Diego, 1985), pp. 290–295, 555–568.
[16] S. M. Sze, *Physics of Semiconductor Devices* (Wiley, New York, 1981), Chap. 14.